Emalie Halifax

Fracture and Fatigue Failures of Products and Components in Service

University of Wales Trinity Saint David
L6 Material Science ACDA 6016

Ordnance, Munitions and Explosives Degree Apprenticeship
Academic Year: 2025 - 2026

Abstract

This case study examines the premature failure of a marine intermediate shaft from a bulk carrier, which fractured in February 2019 after 43,000 hours of service. The investigation employed an integrated approach including Optical Emission Spectroscopy (OES), Scanning Electron Microscopy (SEM), and tensile and Brinell hardness testing.

Findings revealed the primary failure mechanism was fatigue fracture originating from multiple points. Metallurgical analysis identified the root cause to be the use of ASTM 1020 low carbon steel rather than the specified ASTM 1035 steel. This material substitution resulted in a 20% deficiency in ultimate tensile strength (UTS) and a 24% reduction in hardness, significantly lowering the fatigue resistance. Microscopic examination identified deep machining grooves at the fillet root of the flange, which acted as stress concentrations facilitating crack initiation. Consequently, the shaft's safety factor was reduced to 2.22, falling below the required maritime standard of 2.5-5.5.

To prevent recurrence, recommendations include material verification and quality assurance protocols, as well as optimised material surface finishing through final grinding and polishing stages.

Word Count – 3,473

Table of Contents

Abstract i
List of Figures iii
List of Tables iv
List of Equations iv
1 Introduction 1
2 Fatigue Failure in Marine Propeller Shafts 1
2.1 Mechanisms of Fatigue Failure 2
2.1.1 Influence of Stress Concentration and Surface Defects 5
2.2 Fracture Characteristics in Fatigue Failures 6
2.2.1 Macroscopic Features 6
2.2.2 Microscopic Features 9
3 Testing Methodologies in Failure Analysis 10
3.1 Mechanical Testing Methodologies 10
3.1.1 Hardness Testing 10
3.1.2 Tensile Testing 11
3.2 Microscopic Techniques 11
3.3 Chemical Analysis Techniques 12
3.3.1 Optical Emission Spectroscopy 12
3.3.2 Energy Dispersive X-ray Spectroscopy 13
4 Case Study – Bulk Carrier Intermediate Propeller Shaft Failure Analysis 13
4.1 Failure Mechanisms 14
4.1.1 Material Characterisation 16
4.1.2 Mechanical Properties Evaluation 20
4.1.3 Failure Analysis Findings 22
5 Case Study Evaluation 22
5.1 Chemical Evaluation 22
5.2 Mechanical Properties Evaluation 24
5.3 Microscopic and Macroscopic Examination Evaluation 25
6 Conclusion 25
7 Recommendations 26
8 References 27

List of Figures

Figure 2-1 - Combined Loading Conditions Acting on a Ship's Intermediate Shaft During Propulsion 3

Figure 2-2 - Three Stages of Fatigue 4

Figure 2-3 - Schematic Stress Profile Along the Line X-X' Showcasing Increased Stress at Crack Tips, Recreated From [6]..... 5

Figure 2-4 - Macroscopic Characteristics of Fatigue Failure Highlighting (a) The Three Regions Under (b) Unidirectional Bending and (c) Reverse Bending Fatigue [2]..... 7

Figure 2-5 - Macroscopic Features of Fatigue Failure of (a) Marine Propeller Shaft [4] and (b) a Rear Differential Shaft [8] 8

Figure 2-6 - Microscopic Characteristics of Fatigue Failure [2] 9

Figure 4-1 - Failed Bulk Carrier Shaft Highlighting Fracture Location, Compared to New Shaft [4] 13

Figure 4-2 - Schematic of typical propulsion system for a Bulk Carrier [4] 14

Figure 4-3 - Recovered Components of Failed Intermediate Shaft [4] 15

Figure 4-4 - Stereomicroscopic Observation of Fracture Morphology [4] 17

Figure 4-5 - (a) Stereomicroscopy and (b) SEM Observations, on Circled Location on (a), of Machining Marks on Intermediate Shaft [4] 18

Figure 5-1 – Yield Strength, Tensile Strength and Brinell Hardness versus Carbon wt% for Plain Carbon Steels [6] 23

Figure 5-2 – Approximate Values of Brinell (HB), Vickers (HV) and Rockwell C (HRC) Harness, as a Function of Ultimate Tensile Strength for Carbon and Alloy Steels [5] 24

List of Tables

Table 4-1 - Chemical Composition of Shaft Material (wt%) 19

Table 4-2 – Mechanical Properties of Shaft Material 21

List of Equations

2-1 2

2-2 5

4-1 20

1 Introduction

Marine structures are designed to operate safely and reliably over extended service lives, while minimising the likelihood of catastrophic failure. Increasing demand for lightweight structures capable of sustaining higher loads has introduced new challenges [1]. Failures in marine structures may arise from a range of mechanisms including elastic deformation, yielding, fatigue, corrosion and creep, all of which compromise structural integrity and highlight the necessity of systematic failure analysis.

Evaluating these failure mechanisms requires an understanding of the processes leading to failure, their potential consequences and mitigation methods. Testing methods for failure are critical in identifying weaknesses and validating design assumptions. Case studies provide valuable insights into the interaction between design, operational demands and environmental exposure.

Marine structure failures can be categorised into four domains:

- Ship Structural Failures
- Propulsion System Failures
- Off-Shore Structural Failures
- Failures of Marine Equipment

This report focuses on the failure mechanisms of in-service marine propeller shafts and evaluates the testing methodologies applied in subsequent analysis. By examining the underlying causes of failure and effectiveness of diagnostic methodologies, this study seeks to understand how such failures can be mitigated and prevented.

2 Fatigue Failure in Marine Propeller Shafts

Shafts are critical mechanical components of which are essential for transmitting motion and torque to ensure safe, efficient operation. They can be categorised based on the load acting on them: Mandrel and transmission shafts which undergo bending and torque stresses and rotating shafts which are subjected to

fluctuating loads comprising of bending and torque of various degrees of stress concentration [2]. Figure 2-1 [3] illustrates the stresses a rotating propulsion shaft undergoes during navigation, where total stress (σ_{total}) can be expressed as [4]:

$$\sigma_{total} = \sqrt{3\tau^2 + \left(\sigma_{pt} + \sigma_{sw} + \sigma_{ie}\right)^2} \qquad \textbf{2-1}$$

Where τ is the torsional tangential stress, σ_{pt} is the axial stress (either compressive or tensile) transferred from the propeller thrust, σ_{sw} is the bending stress from the self-weighting of the shaft and σ_{ie} is bending stress from installation error.

Fluctuating loads on a propulsion shaft during operation is a key driver of fatigue failure, which is the most common failure mechanism for shafts under normal working conditions [5].

2.1 Mechanisms of Fatigue Failure

Fatigue occurs when materials are subjected to dynamic and fluctuating stresses [6] over a period of time. Due to repeated stress cycling, it is possible for failure to occur at a stress level considerably lower than the tensile or yield strength of a material. The three stages of fatigue presented in Figure 2-2 are:

1. Crack Initiation
2. Crack Propagation
3. Final Fracture

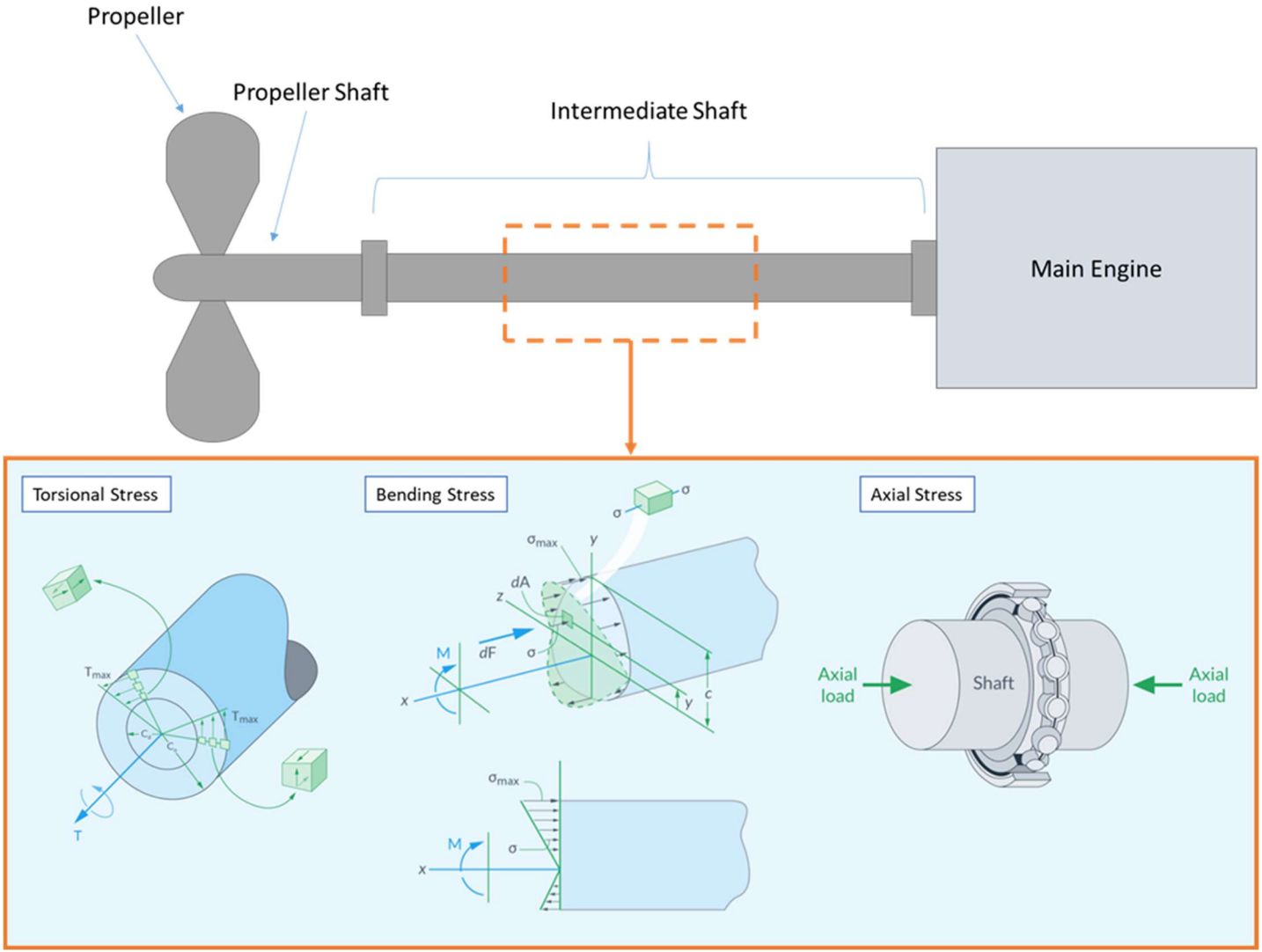

Figure 2-1 - Combined Loading Conditions Acting on a Ship's Intermediate Shaft During Propulsion

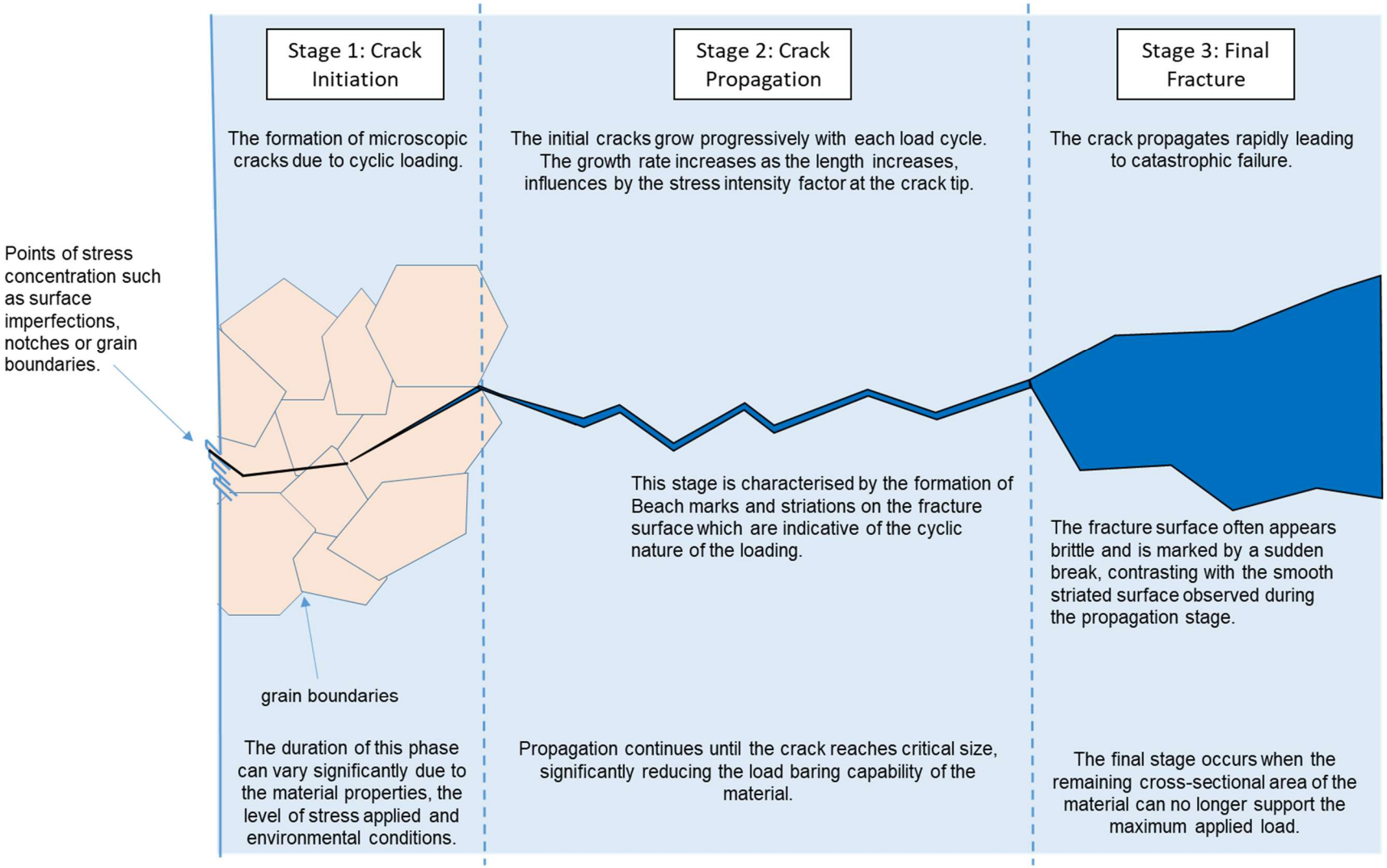

Figure 2-2 - Three Stages of Fatigue

2.1.1 Influence of Stress Concentration and Surface Defects

Microscopic defects, often called stress raisers, play a key role in fatigue failure as they create localised regions of elevated stress [6]. This phenomenon is demonstrated in Figure 2-3 which shows that the magnitude of localised stress decreases with distance from the crack tip. If it is assumed that the crack is similar to an elliptical hole and the load is applied perpendicular to the crack, the maximum stress σ_m, at the crack tip can be approximated by [5, 6]:

$$\sigma_m = 2\sigma_o \left(\frac{a}{\rho_t}\right)^{\frac{1}{2}} \qquad \textbf{2-2}$$

Where σ_o is the magnitude of the nominal applied tensile stress, ρ_t is the crack radius and a is the length of a surface crack or half the length of an internal crack.

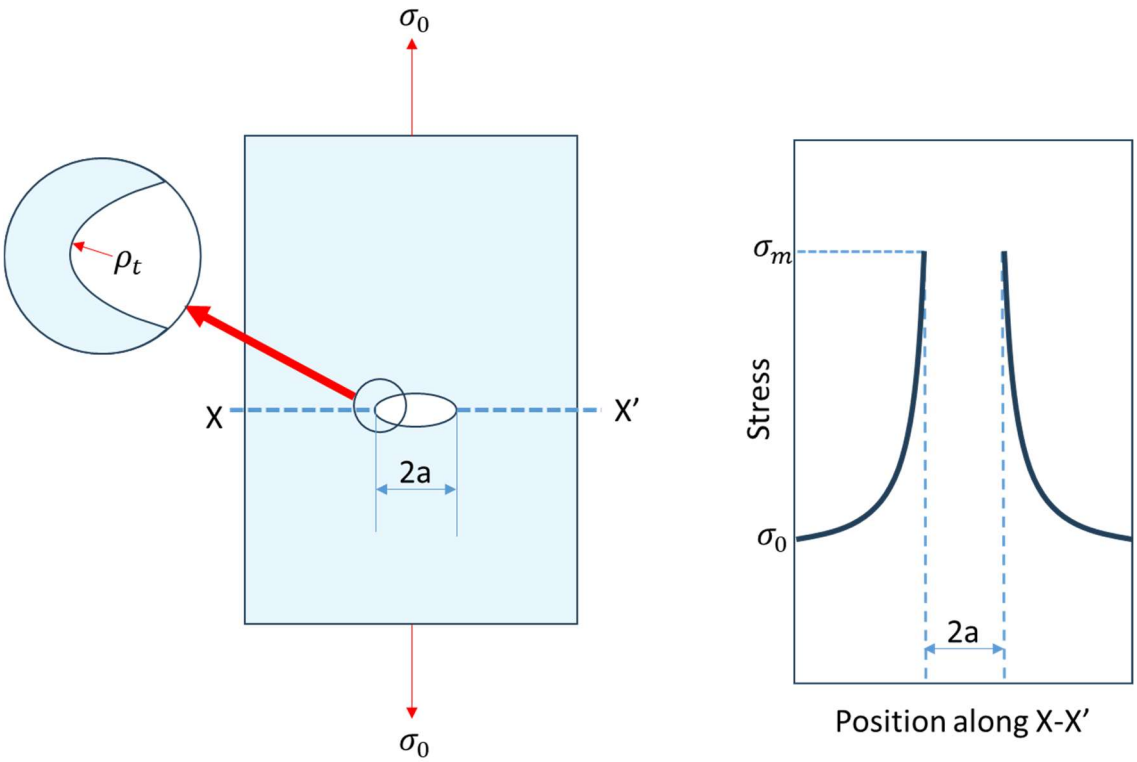

Figure 2-3 - Schematic Stress Profile Along the Line X-X' Showcasing Increased Stress at Crack Tips, Recreated From [6]

Areas of localised stress promote large plastic deformation zones in metals at the crack tips [5], along with early crack initiation. Stress concentration is not

restricted to microscopic defects; it can also be present in macroscopic internal discontinuities [6].

2.2 Fracture Characteristics in Fatigue Failures

Fatigue failure leaves a distinct macroscopic and microscopic signature on the fracture surface. These features provide critical insight into loading conditions, stress concentration and material behaviour. Subsequent analysis aids the identification of failure modes and validation of fatigue life predictions.

2.2.1 Macroscopic Features

At the macroscopic level, fatigue fractures exhibit distinct features which reflect the progressive nature of crack initiation and growth and can be divided into three regions:

1. Crack initiation
2. Crack propagation
3. Rapid fracture

The relative positions and structure of these regions are closely related to the cyclic loading acting on the shaft [2] as illustrated in Figure 2-4. The presence of beach marks is a key identifier of high-cycle fatigue and can highlight crack initiation points. This area is typically smooth and flat, contrasting with the rough, brittle texture of the rapid fracture region [2] as shown in Figure 2-5. Ratchet marks also indicate multiple initiation points and areas of high stress concentration [7].

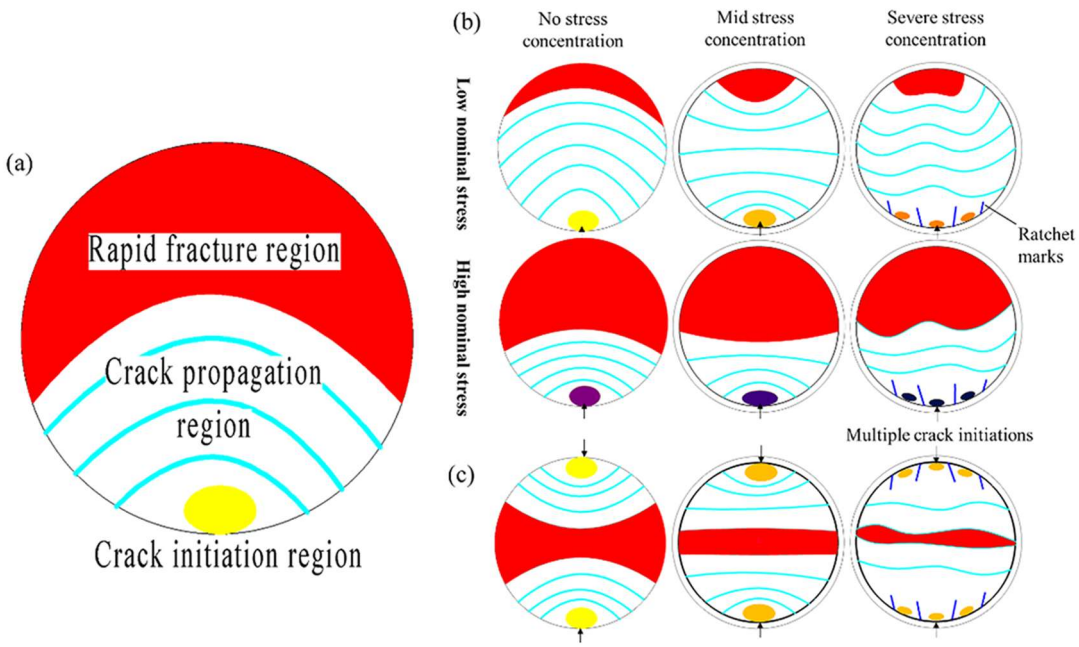

Figure 2-4 - Macroscopic Characteristics of Fatigue Failure Highlighting (a) The Three Regions Under (b) Unidirectional Bending and (c) Reverse Bending Fatigue [2]

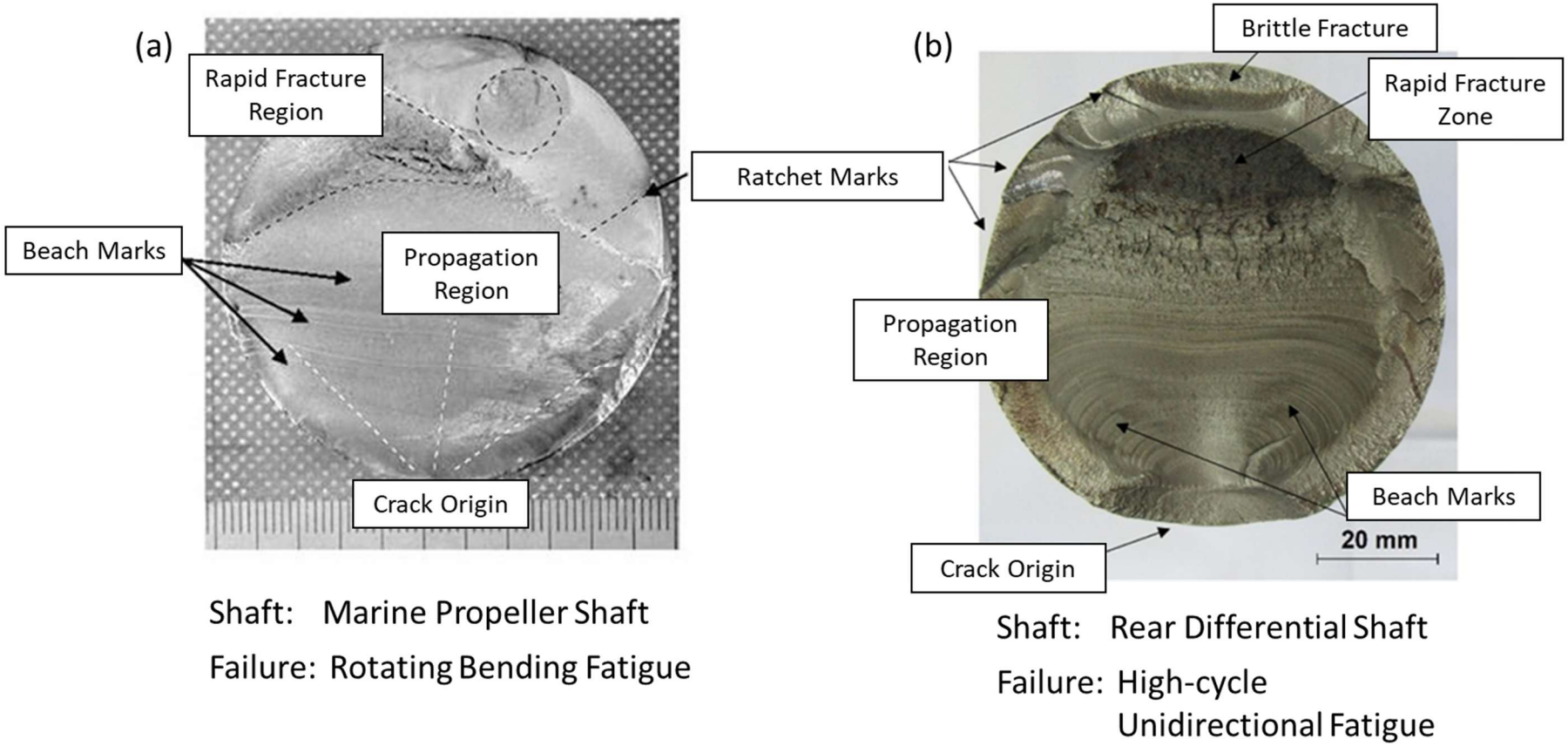

Figure 2-5 - Macroscopic Features of Fatigue Failure of (a) Marine Propeller Shaft [4] and (b) a Rear Differential Shaft [8]

2.2.2 Microscopic Features

Microscopic examination allows further analysis of the underlying mechanisms governing fatigue crack growth. Resulting from the repeated blunting and sharpening of the crack tip striations form a microscopic fingerprint of the cyclic loading on the shaft [7]. The spacing between markings can provide an indication of the propagation rate of the crack per load cycle. The microstructure and grain boundaries of a material can vary the morphology of the fatigue striations [2].

Additional features such as radial ridges and grinding marks can be identified at the crack initiation sites, while dimple-like features can be observed at the final fracture region [2]. These are highlighted in Figure 2-6.

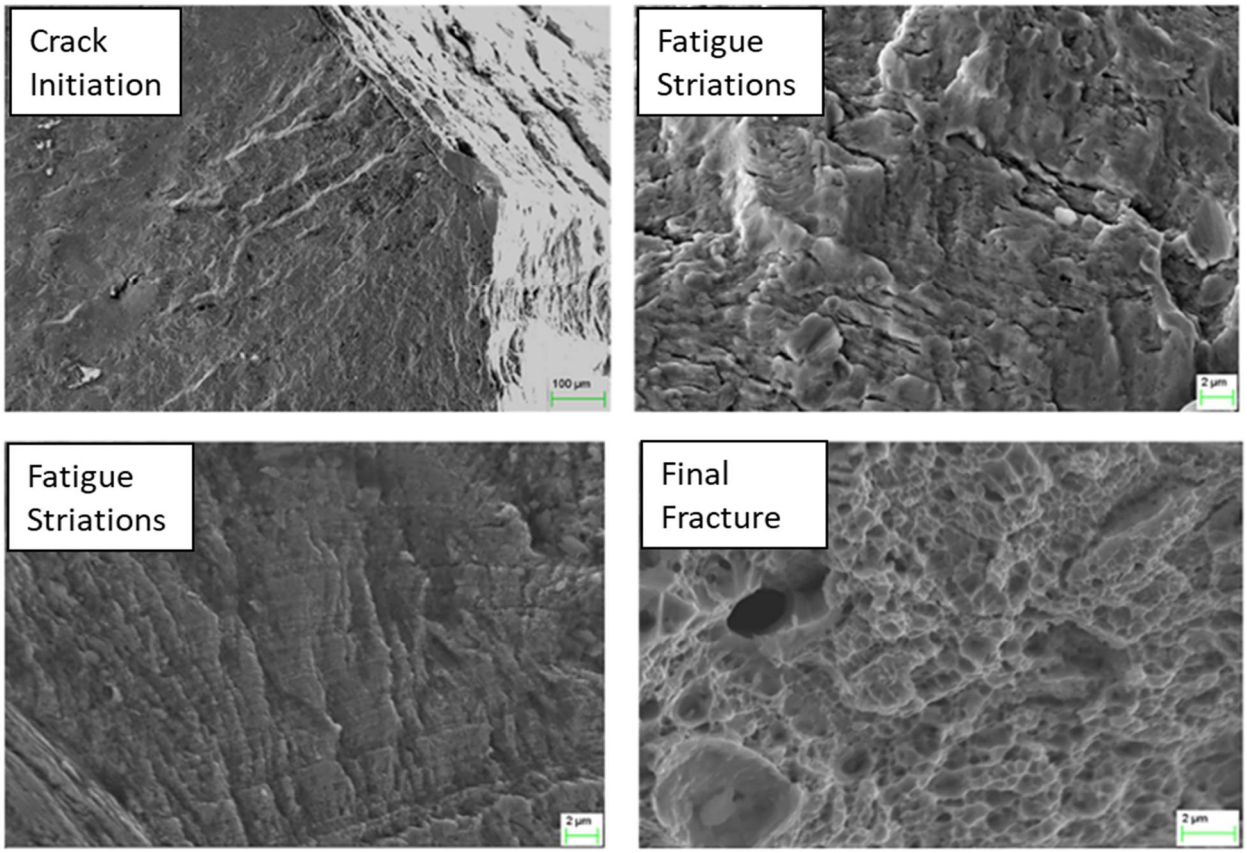

Figure 2-6 - Microscopic Characteristics of Fatigue Failure [2]

3 Testing Methodologies in Failure Analysis

Failure analysis requires an integrated approach that combines mechanical property evaluation with detailed microstructural and chemical characterisation to accurately identify root causes and predict material performance under service conditions.

3.1 Mechanical Testing Methodologies

3.1.1 Hardness Testing

Hardness is defined as a material's resistance to permanent, localised plastic deformation under applied contact stresses. It is typically quantified through indentation-based tests that reflect its underlying microstructural strengthening mechanisms. The depth of the indentation reflects the hardness of the material, with softer materials having a larger indentation and a lower hardness value [6].

Hardness is typically assessed using standardised methodologies such as the Rockwell, Vickers and Brinell tests. Each employs different indentation geometry and measurement approaches, allowing hardness to be evaluated across a wide range of materials and microstructural conditions.

3.1.1.1 Rockwell Hardness Test

The Rockwell test is the most common method [6] and measures hardness by determining depth of penetration of an indenter under minor and major loads. Rockwell's versatility lies in its ability to use either a diamond cone or steel ball indenter under varying load conditions. The choice of indenter and applied load corresponds to specific Rockwell scales, such as HRC, HRB and HRF, to allow accurate hardness measurements across hard and soft metallic materials [9].

3.1.1.2 Brinell Hardness Test

The Brinell hardness test employs a hardened steel or carbide ball to apply a substantial load onto the material surface [5, 6]. Standard practice uses a 10mm diameter indenter under loads ranging from 500-3000kg, applied for a specific period [10]. The resulting indentation is used to calculate the Brinell Hardness Number (HB) to provide a measure of the material's hardness.

3.1.1.3 Vickers Hardness Test

A 136° angle diamond pyramidal indenter is employed in the Vickers hardness test, which derives results from the diagonal length of the indentation under a single test load [11]. As the geometry is constant, the Vickers number is independent of the load making it suitable for very hard materials and microhardness testing.

3.1.2 Tensile Testing

When a uniform load is applied over a cross-sectional area and remains static or varies gradually, a standard tensile stress-strain test can be performed to determine key mechanical properties such as yield strength, ultimate tensile strength (UTS) and elastic modulus [6]. These properties are critical in fatigue and fracture analysis as they define the material's load-bearing capacity, indicate its resistance to crack initiation and propagation, while providing baseline data for assessing whether operational stresses exceed design safety limits.

During a tensile test, a load is applied uniaxially along the longitudinal axis of a standardised specimen [12]. While the primary mode applies tension, other loading configurations for compression and shear can be applied. Certain applications may require torsional loading to evaluate material behaviour under combined stress states [6].

3.2 Microscopic Techniques

Microscopic evaluation is critical in failure analysis [6], enabling identification of detailed microscopic fracture features. Optical microscopy is an essential preliminary technique in fatigue and fracture analysis, providing low-to-medium magnification of fracture surfaces with the use of visible light [6]. This is beneficial for identifying macroscopic features and is often used for mapping crack paths and distinguishing between fatigue and final overload regions.

For microscopic analysis, electron microscopy is often employed. Electron microscopy encompasses advanced imaging techniques that use a focused beam of electrons to characterise the surface and internal structure of materials

[13]. Due to the short wavelength, electron microscopes can resolve features at micro and nanoscale dimensions.

The most common form of electron microscopy is Scanning Electron Microscopy (SEM), which scans the material surface with an electron beam. The reflected or backscattered electron beam is collected to produce a high-resolution image [6, 13]. SEM can be used at magnifications ranging from 10X to 50,000X [6], making it indispensable for identifying fatigue striations, crack initiation sites and microstructural defects.

3.3 Chemical Analysis Techniques

Chemical analysis plays a vital role in failure analysis as many material failures originate from variations in chemical composition, contamination, improper alloying and environmental degradation [14]. Understanding the chemical composition of a failed component can determine if a material met specifications, contained impurities or if environmental conditions contributed to crack initiation and propagation. Chemical analysis, therefore, complements mechanical and fractographic evaluations by revealing compositional factors that may have influenced fatigue resistance, fracture toughness or overall structural integrity.

3.3.1 Optical Emission Spectroscopy

Optical Emission Spectroscopy (OES) is a widely used technique for bulk chemical analysis of metallic materials and alloys. The process involves generating a high energy electrical spark [15] on the sample surface, which excites the atoms causing them to produce characteristic optical emissions. By measuring the intensity of these emissions, the chemical composition of the sample can be accurately determined. OES is particularly useful in failure analysis to verify alloy grades, detect off-specification elements and identify trace impurities which can contribute to embrittlement or reduce fatigue performance. Its ability to analyse a wide range of metallic elements make it a standard tool in metallurgical evaluations.

3.3.2 Energy Dispersive X-ray Spectroscopy

Energy Dispersive X-ray Spectroscopy (EDS or EDX) is a microanalytical technique commonly used with SEM to provide localised chemical composition data at the microstructural scale. During SEM imaging, characteristic x-rays are generated as the electron beam interacts with the specimen. These x-rays have element specific characteristics enabling identification of the chemical composition of specific features such as inclusions, precipitates, corrosion products or fracture surface deposits [14]. In fatigue and fracture analysis, EDS is particularly valuable for identifying non-metallic inclusions that act as crack initiation sites, detecting environmental contaminates that promote stress-corrosion cracking and characterising secondary phases that influence crack propagation.

4 Case Study – Bulk Carrier Intermediate Propeller Shaft Failure Analysis

In February 2019, a failure occurred on a bulk carrier while performing berthing manoeuvres at half speed. When attempting to engage “dead slow” for final positioning, the crew reported a total loss of rudder effect and suction. Subsequent inspection found that the intermediate shaft fractured at the fillet root of the flange [4]. Figure 4-1, shows the failed shaft compared to a new shaft.

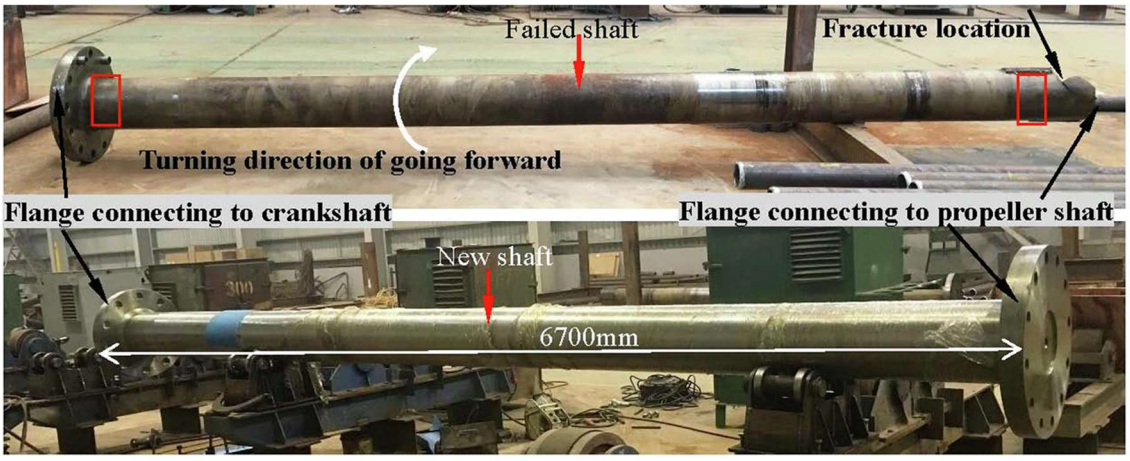

Figure 4-1 - Failed Bulk Carrier Shaft Highlighting Fracture Location, Compared to New Shaft [4]

The intermediate shaft connected the crankshaft to the propeller shaft as demonstrated in Figure 4-2. This measured 6700mm in length and 340mm in diameter with two flanges 83mm thick and 810mm in diameter. The shaft was manufactured in 2007 and had been in service for 43,000 hours before fracturing.

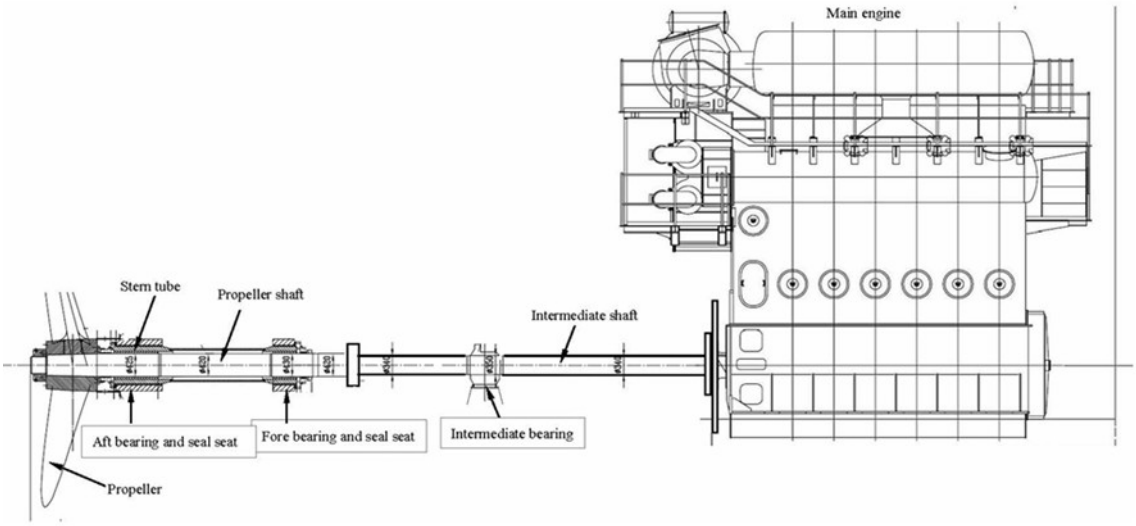

Figure 4-2 - Schematic of typical propulsion system for a Bulk Carrier [4]

4.1 Failure Mechanisms

From initial macroscopic analysis of the recovered flange and shaft, four main crack propagation zones, labelled A, B, C and D on Figure 4-3, with a singular final fracture zone indicated in (a), were identified. Ratchet marks indicate multiple crack initiation points along with high stress concentration and torsional loading on the shaft. The final fracture zone accounts for 8% of the total fracture surface, indicating the shaft was under minimal static load at the time of failure.

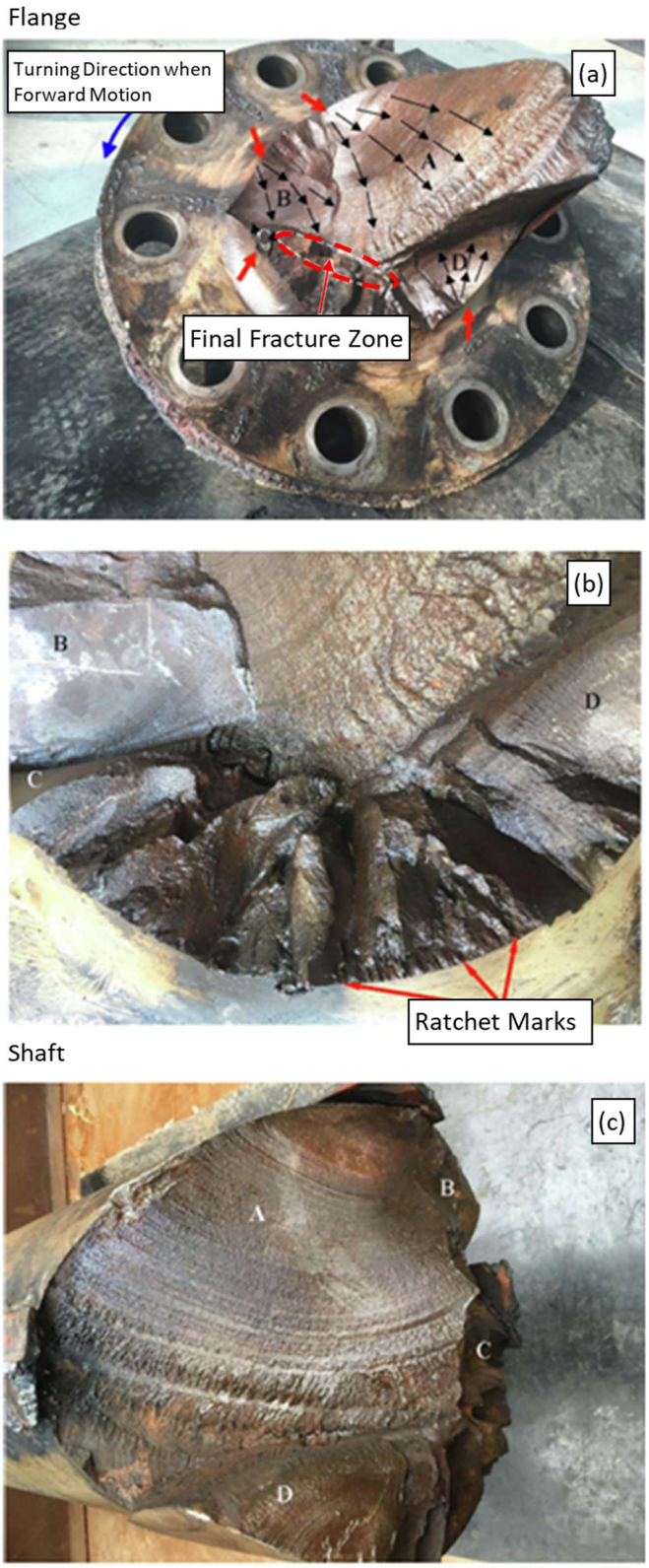

Figure 4-3 - Recovered Components of Failed Intermediate Shaft [4]

Bach marks, highlighted in Figure 4-4, distinctly suggest fatigue failure leading to the final fracture. Following beach marks, crack initiation points can be identified, along with the direction of crack propagation indicated by the red arrows in Figure 4-4(a)(c)(e) and (f). The crack origins were initiated from the fillet root of the flange and propagated outward [4]. It can be shown that cracks propagated towards the central zone at an angle of 45-55° of the shaft axis. The fracture angles of the cracks are negative and positive to the shaft axis, suggesting the shaft experienced stresses in both directions during its service. The 55° angle at crack B indicates the dominant failure was due to torsional and bending tension.

Figure 4-4(h) highlights a groove 44mm from the flange plane. This coincides with crack origin locations, which suggest that there is a weakness in the groove that led to the shaft failure. Further analysis was undertaken on samples of the flange fillet regions. Stereomicroscope observation identified machining marks on the fillet roots, SEM revealed these marks were notably deep with short cracks at the bottom as highlighted in Figure 4-5. These notches could act as areas of significant stress concentrations providing effective initiation areas for fatigue.

4.1.1 Material Characterisation

Chemical composition of the intermediate shaft was determined using OES with samples from the crack origins and flange connected to the crankshaft. The design drawings state the shaft was to be made of ASTM 1035 steel with variance expected within a specified range due to is large size. Table 4-1 shows the carbon content of the shaft was 0.19-0.24 wt%, considerably lower than the required 0.32-0.40 wt% of ASTM 1035 steel. This indicates that the failed shaft was constructed of low carbon ASTM 1020 steel, with a lower carbon content at the flange region close to the failure point. Lower carbon levels negatively affect the fatigue strength of materials.

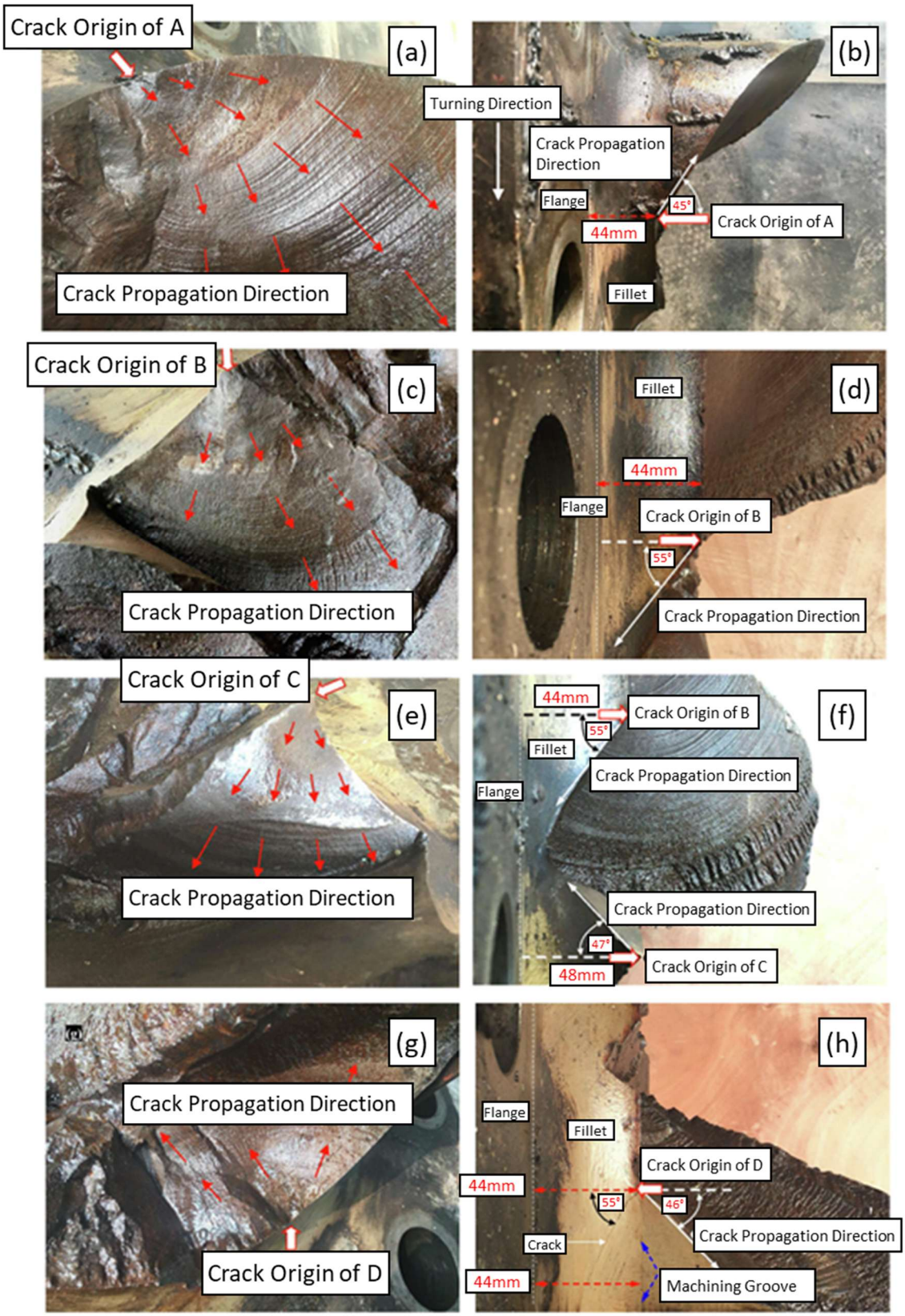

Figure 4-4 - Stereomicroscopic Observation of Fracture Morphology [4]

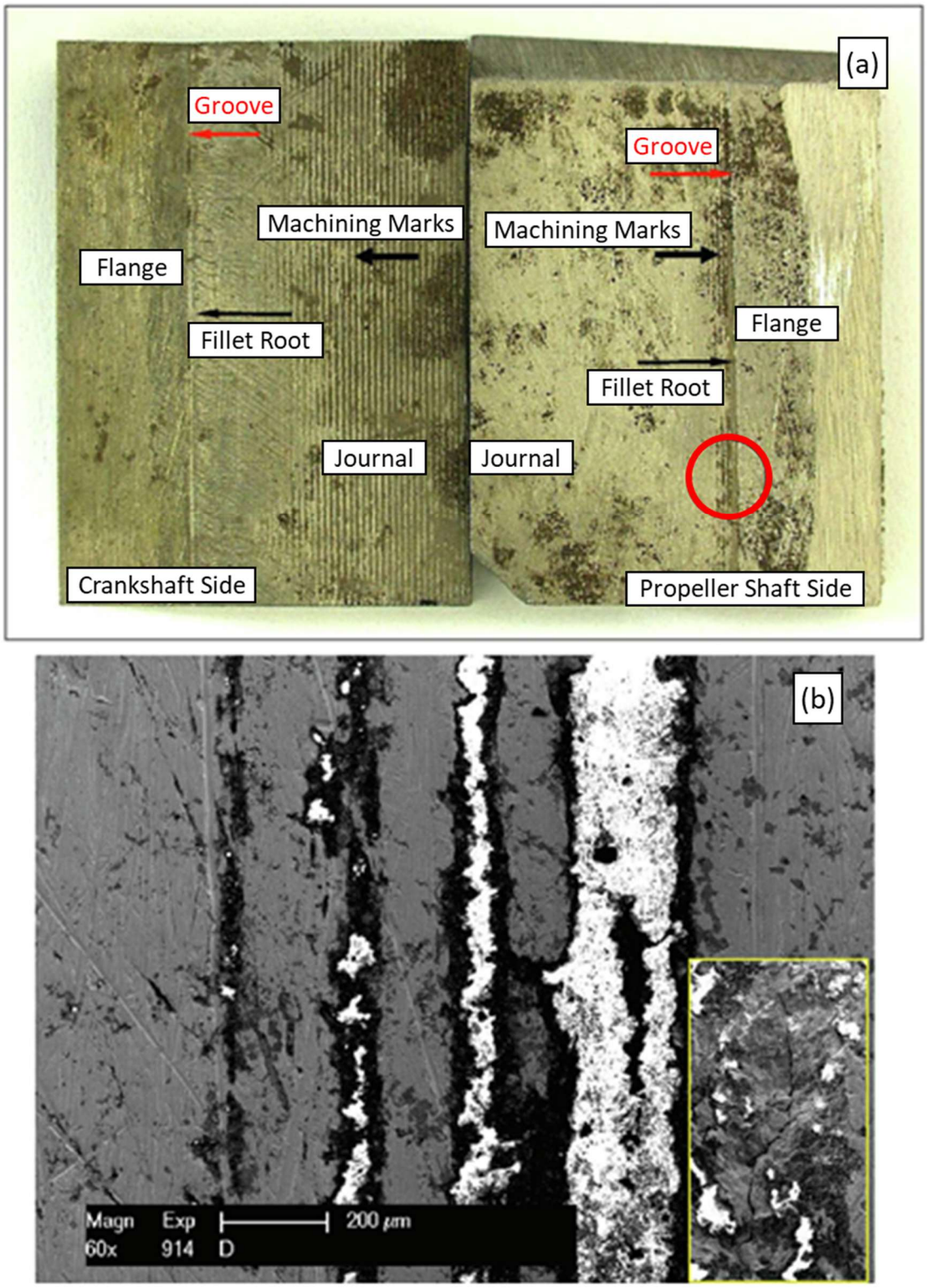

Figure 4-5 - (a) Stereomicroscopy and (b) SEM Observations, on Circled Location on (a), of Machining Marks on Intermediate Shaft [4]

Table 4-1 - Chemical Composition of Shaft Material (wt%)

Examination Location		C	Si	Mn	P	S	Cr	Ni	Cu
Flange connected to propulsion shaft	Crack origin A	0.19	0.23	0.60	0.007	0.003	0.09	0.05	0.12
	Crack Origin B	0.20	0.23	0.59	0.006	0.004	0.09	0.05	0.12
	Crack Origin C	0.19	0.24	0.60	0.007	0.004	0.009	0.05	0.12
	Crack Origin D	0.19	0.24	0.59	0.007	0.005	0.009	0.05	0.11
Flange connected to crankshaft	Location 1	0.24	0.24	0.63	0.008	0.004	0.09	0.05	0.12
	Location 2	0.24	0.24	0.63	0.008	0.004	0.09	0.05	0.12
	Location 3	0.24	0.25	0.64	0.008	0.004	0.09	0.05	0.12
ASTM 1020		0.17-0.24	0.17-0.37	0.35-0.65	≤0.0035	≤0.0035	≤0.25	≤0.25	≤0.25
ASTM 1035		0.32-0.40	0.17-0.37	0.50-0.80	≤0.0035	≤0.0035	≤0.25	≤0.25	≤0.25

4.1.2 Mechanical Properties Evaluation

4.1.2.1 Hardness Testing

The Brinell test was conducted to determine the macro-hardness of the shaft with a load of 250kg and a carbide indenter 5mm in diameter. Twenty readings were taken with an average hardness value of HB114, 24% lower than the specified lower limit of HB150-185.

4.1.2.2 Tensile Testing

Tensile testing was conducted using an Instron-5500R tensile tester and standard round specimens of 50mm in length and 10mm in diameter, taken from the marked location in Figure 4-1. From the results in Table 4-2, it can be seen the UTS and yield strength were lower than technical specification requirements, while the elongation and reduction areas were within tolerance. The UTS and yield strength close to the point of fracture were 20% and 16% lower than the required values, however, the samples from the crankshaft flange were 8% and 7% lower, coinciding with the difference in material composition of the shaft. During evaluation of the results, it was noted that the average UTS near the crack origins (416 MPa) was 12% lower than the lower limit of the UTS based on the design criteria (520 MPa).

Failure analysis of the UTS (σ_s) determined that the shaft did not have the appropriate safety factor (K), which was determined by 4-1.

$$K = \frac{\sigma_s}{\sigma_{total}} \qquad \textbf{4-1}$$

The permitted maritime safety factor for rigid transmission shafts is 2.5-5.5 [4], whereas the flange near the propeller shaft and the crankshaft had safety factors of 2.22 and 2.43 respectively.

The low mechanical properties are linked to low carbon levels in the material.

Table 4-2 – Mechanical Properties of Shaft Material

Sampling Location		Sample Number	Yield Strength, MPa	Ultimate Yield Strength, MPa	Elongation, %	Reduction Area, %
Close to flange connecting to propeller-shaft (near fracture)	Axial Sample	1	220	441	42.0	63.1
		2	220	428	35.4	63.0
	Transverse Sample	3	215	412	34.9	60.5
		4	217	409	34.0	60.5
	Tangential Sample	5	219	419	39.9	62.8
		6	220	417	40.0	59.4
	Average		219	416	37.7	61.6
Close to flange connecting to crankshaft	Axial Sample	1	241	452	33.9	59.9
		2	235	442	33.4	60.8
	Transverse Sample	3	241	456	29.2	59.1
		4	235	440	33.5	59.7
	Tangential Sample	5	238	439	34.1	58.1
		6	237	446	32.5	55.7
	Average		238	446	32.8	58.9
Technical Specification			≥260	≥520	≥15-≥21	≥30-≥45

4.1.3 Failure Analysis Findings

Through the failure analysis it was concluded that the intermediate shaft failed due to a fatigue fracture. The small fracture zone indicated that the shaft was operating under low stress. Material chemical analysis concluded the material was not of the correct standard for shaft operation, reducing its mechanical properties. The dominant failure mechanism was identified to be the multiple fatigue origins, with all four larger crack initiations occurring from the fillet root flange. Increased stress concentrations were a result of deep machining grooves. Ultimately, the lower carbon levels in the material promoted fatigue crack propagation which, combined with dominant torsional stresses, lead to the shaft's failure.

5 Case Study Evaluation

5.1 Chemical Evaluation

OES confirmed the chemical composition of the material and revealed the shaft was manufactured from ASTM 1020 steel rather than the required ASTM 1035. While OES accurately determined the elemental composition, it did not reveal specific microstructural characteristics such as exact pearlite fraction, grain size or inclusion morphology which influence fatigue performance. OES should be complemented with metallographic examination to assess microstructural features.

Based on the lower carbon content of ASTM 1020 steel, there would have been an increase in soft ferrite (α-Iron) and a reduced fraction of pearlite, which consists of layers of ferrite and cementite (Fe_3C). Cementite is significantly harder but more brittle than ferrite, therefore, increasing the Fe_3C fraction in a steel alloy, while maintaining microstructural elements, enhances hardness and strength in a material [6]. The reduction of pearlite and consequently cementite, directly lowered the material's inherent strength. Comparative mechanical property data indicates that replacing ASTM 1035 with ASTM 1020 typically reduces the UTS

by approximately 20-30% [16, 17]. This is consistent with the measured 20% reduction in the failed shaft. Lower UTS values are characteristic of low carbon steel as demonstrated in Figure 5-1. Ferrite-rich microstructures accelerate fatigue crack propagation because the soft ferrite deforms easily and has fewer microstructural barriers than pearlite [18]. Ultimately, the use of low carbon steel resulted in inadequate tensile performance and reduced resistance to fatigue crack growth, contributing to the shaft's failure.

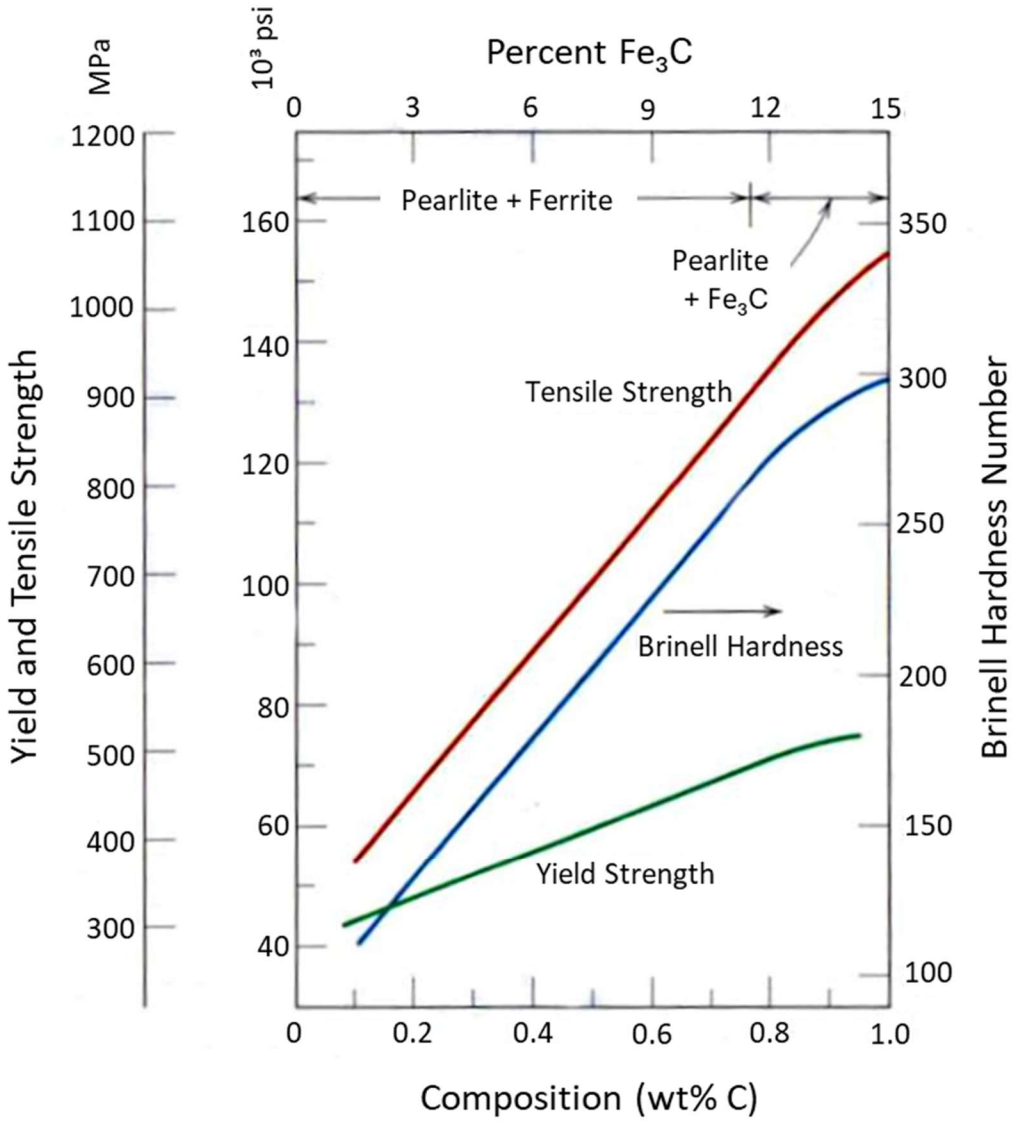

Figure 5-1 – Yield Strength, Tensile Strength and Brinell Hardness versus Carbon wt% for Plain Carbon Steels [6]

5.2 Mechanical Properties Evaluation

Mechanical testing conducted on the intermediate shaft showed the material had significantly reduced strength relative to the design specification. The measured average hardness of HB114, which was 24% lower than the specified requirement, indicates a substantially softer microstructure with reduced resistance to localised plastic deformation. Brinell hardness correlates strongly with yield strength as presented in Figure 5-2. A hardness deficit of this magnitude implies that the material's pearlite and ferrite levels were significantly lower than intended, allowing larger cyclic plastic zones to form at stress concentrations. The reduced hardness therefore facilitated earlier, and more extensive, plastic deformation at the crack origins. This lowered the threshold for microcrack initiation and accelerated the transition to stable crack propagation, making the material more susceptible to fatigue crack initiation under operational loading.

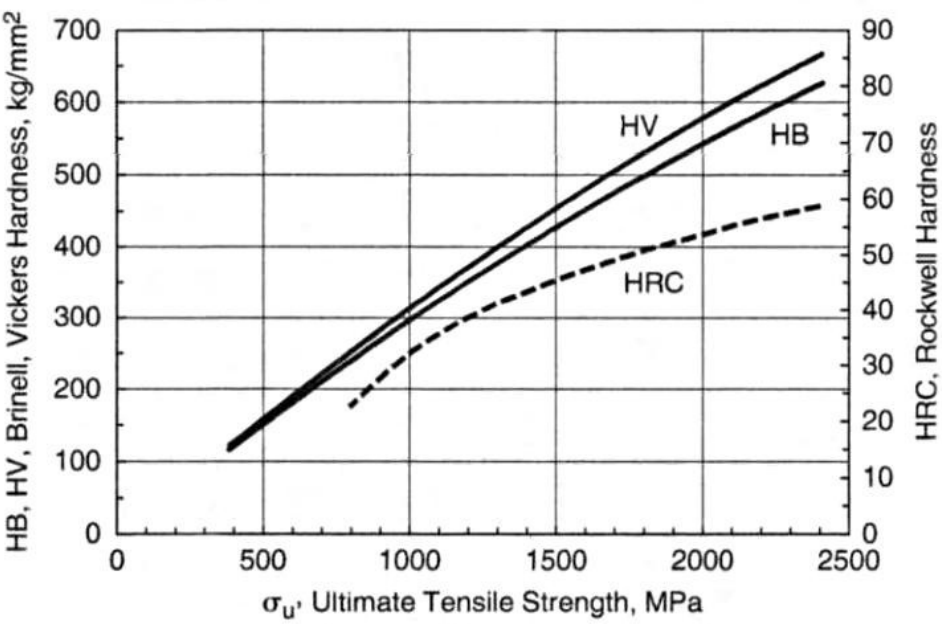

Figure 5-2 – Approximate Values of Brinell (HB), Vickers (HV) and Rockwell C (HRC) Harness, as a Function of Ultimate Tensile Strength for Carbon and Alloy Steels [5]

5.3 Microscopic and Macroscopic Examination Evaluation

Macroscopic and microscopic examinations identified key characteristics of fatigue failure such as striations, crack initiation sites and a relatively smooth crack propagation region. SEM provided high resolution images of the crack origins, enabling identification of notches in the fillet roots. The notches would have produced an area of local peak stress several times the nominal stress levels [6], accelerating crack initiation and fatigue.

SEMs limited field of view restricted its ability to assess the microstructure across the whole fracture surface and the failed shaft. Further assessment of the material structure would have been beneficial in evaluating ferrite and pearlite balance, grain size and inclusion content, while micro-Vickers harness mapping could identify soft zones near the crack origins.

6 Conclusion

The systematic investigation into the failure of the bulk carrier intermediate shaft confirms that the component failed due to a fatigue fracture with multiple origins after 43,000 hours of service. The failure was driven by use of below specification material and machining errors. The key findings include:

- **Out of Specification Material** – Chemical composition testing by OES confirmed the shaft was manufactured using ASTM 1020 low carbon steel instead of the specified ASTM 1035 steel. This substitution resulted in a 20% UTS deficiency and a 24% reduction in hardness, which significantly lowered the materials fatigue threshold and safety factor.
- **Stress Concentration** – Microscopic examination by SEM identified deep machining grooves at the fillet root of the flange. These grooves served as effective stress raisers, facilitating the initiation of multiple cracks.
- **Failure Progression** – The presence of beach and ratchet marks confirmed high-cycle fatigue while the relatively small final fracture zone proved the shaft was operating under minimal static load at the time of ultimate failure.

7 Recommendations

To prevent premature fatigue failure of marine propulsion shafts and to ensure structural integrity over long service lives, the following recommendations should be implemented:

- **Stringent Material Quality Assurance** – A root cause of the failure discussed in this report was the use of below specification steel. Use of OES and hardness testing during manufacture and at point of delivery would ensure the carbon content and, ultimately, the UTS meets minimum design specifications before the shaft enters service.
- **Optimisation of Manufacturing Finish** – Machining grooves in the fillet root of the flange were identified as a primary site for multiple crack origins. Manufacturing processes should ensure there is a final grinding and polishing stage to remove all circumferential notches.
- **Enhanced In-Service Monitoring** – Given the high-cycle nature of the failure, routine inspections should utilise enhanced techniques to enable identification of stable fatigue cracks before they reach the critical size for catastrophic failure.

8 References

[1] G. Vukelić and G. Vizentin, “Common Case Studies of Marine Structural Failures,” in *Failure Analysis and Prevention*, InTech, 2017.

[2] N. Hou, N. Ding, S. Qu, W. Guo, L. Liu, N. Xu, L. Tian, H. Xu, X. Chen, F. Zairi and C.-M. L. Wu, “Failure modes, mechanisms and causes of shafts in mechanical equipment,” *Engineering Failure Analysis,* vol. 136, 2022.

[3] C. Young, “Stresses in a Shaft: Understanding the Mechanics,” [Online]. Available: https://engineerexcel.com/stresses-in-a-shaft/. [Accessed 5 January 2026].

[4] X.-l. Hx and Z.-w. Yu, “Failure analysis of a marine intermediate shaft,” *Engineering Failure Analysis,* no. 126, 2021.

[5] N. E. Dowling, S. L. Kampe and M. V. Kral, Mechanical Behaviour of Materials: Engineering Methods for Deformation, Fracture and Fatigue, 5th ed., Harlow: Pearsons, 2020.

[6] J. William F. Callister and D. G. Rethwisch, Materials Science and Engineering, Global ed., John Wiley & Sons, 2020.

[7] G. Pantazopoulos and S. Papaefthymiou, “Failure and Fracture Analysis of Austenitic Stainless Steel Marine Propeller Shaft,” *Journal of Failure Analysis and Prevention,* pp. 762-767, 2015.

[8] T. F. Azevedo, W. R. V. Sampaio, E. C. B. Câmara, G. D. Lima, W. F. d. S. Silva and S. d. S. Ramos, “Failure analysis of a surgarcane loader rear shaft,” *Engineering Failure Analysis,* vol. 109, 2020.

[9] *ASTM E18-15 - Standard Test Methods for Rockwell Hardness of Metallic Materials,* ASTM International =, 2015.

[10] *ASTM E10-12 - Standard Test Method for Brinell Hardness of Metalic Materials,* ASTM International, 2012.

[11] *ASTM E92-16 - Standard Test Methods for Vickers Harndess and Knoop Hardness of Metalic Materials,* ASTM Imternational, 2016.

[12] *ASTM E8/E8M-22 - Standard Test Methods for Tension Testing of Metalic Materials,* ASTM International, 2022.

[13] Thermo Fisher Scientific, “SEM Technology: A Comprehensive Guide”.

[14] Thermal Fisher Scientific, “Manufacturing Failure Analysis woth Energy-Dispersive Spectroscopy,” [Online]. Available: https://www.thermofisher.com/uk/en/home/materials-science/learning-center/eds-analysis/manufacturing-failure-analysis.html. [Accessed 5 January 2026].

[15] Thermal Fisher Scientific, “Optical Emission Spectroscopy (OES) Academy,” [Online]. Available: https://www.thermofisher.com/uk/en/home/industrial/spectroscopy-elemental-isotope-analysis/spectroscopy-elemental-isotope-analysis-learning-center/elemental-structural-analysis-information/oes-academy.html. [Accessed 29 December 2025].

[16] “AISI 1020 Steel,” [Online]. Available: https://matweb.com/search/DataSheet.aspx?MatGUID=a2eed65d6e5e4b66b7315a1b30f4b391&ckck=1. [Accessed 29 December 2025].

[17] “AISI 1035 Steel,” [Online]. Available: https://www.matweb.com/search/DataSheet.aspx?MatGUID=cea798a6f9f64a20b8813f3c35f70df3. [Accessed 29 December 2025].

[18] M. Li, F. Sun, D. Li, P. E. O'Donoghue, S. B. Leen and N. P. O'Dowd, “The effect of ferrite phases on the micromechanical reponse and crack intiation in the inter-critical head-affected zone of a welded 9Cr martensitic steel,”

Fatigue & Fracture of Engineering Materials & Structures, vol. 41, no. 6, pp. 1245-1259, 2018.